Gerda

Progress report to the LNGS scientific committee

(Appendix)

LNGS-EXP 33/05 add. 10/10

This Gerda report summarizes the progress achieved during the last six months. A *Short Write-up* is linked at:

`http://www.mpi-hd.mpg.de/GERDA/reportsLNGS/gerda-lngs-sc-apr10-shwup.pdf`.

Experimental and technical details are given in the *Appendix* which is linked at:

`http://www.mpi-hd.mpg.de/GERDA/reportsLNGS/gerda-lngs-sc-apr10-appdx.pdf`.

Previous reports are available at: `http://www.mpi-hd.mpg.de/GERDA/reportsLNGS`.

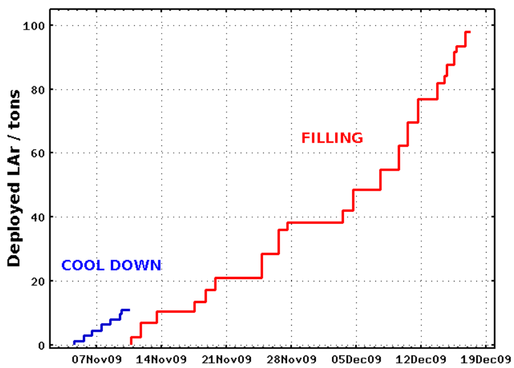

April 2010

H. Aghaei [m], M. Agostini [f], M. Allardt [c], A.M. Bakalyarov [l], M. Balata [a], I. Barabanov [j], M. Barnabe-Heider [f], L. Baudis [q], C. Bauer [f], N. Becerici-Schmid [m], E. Bellotti [g,h], S. Belogurov [k,j], S.T. Belyaev [l], A. Bettini [n,o], L. Bezrukov [j], V. Brudanin [d], R. Brugnera [n,o], D. Budjas [f], A. Caldwell [m], C. Cattadori [g,h], F. Cossavella [m], E.V. Demidova [k], A. Denisiv [j], A. Di Vacri [a], A. Domula [c], A. D'Andragora [a], V. Egorov [d], A. Ferella [q], K. Freund [p], F. Froborg [q], N. Frodyma [b], A. Gangapshev [j], A. Garfagnini [n,o], S. Gazzana [f,a], R. Gonzalea de Orduna [e], P. Grabmayr [p], K.N. Gusev [l,d], V. Gutentsov [j], W. Hampel [f], M. Heisel [f], S. Hemmer [m], G. Heusser [f], W. Hofmann [f], M. Hult [e], L. Iannucci [a]. L.V. Inzhechik [j], J. Janicsko [m], J. Jochum [p], M. Junker [a], S. Kionanovsky [j], I.V. Kirpichnikov [k], A. Klimenko [d,j], M. Knapp [p], K-T. Knoepfle [f], O. Kochetov [d], V.N. Kornoukhov [k,j], V. Kusminov [j], M. Laubenstein [a], V.I. Lebedev [l], B. Lehnert [c], D. Lenz [m], S. Lindemann [f], M. Lindner [f], I. Lippi [o], X. Liu [m], B. Lubsandorzhiev [j], B. Majorovits [m], G. Meierhofer [p], I. Nemchenok [d], L. Pandola [a], K. Pelczar [b], F. Potenza [a], A. Pullia [i], S. Riboldi [i], F. Ritter [p], C. Rossi Alvarez [o], R. Santorelli [q], J. Schreiner [f], B. Schwingenheuer [f], S. Schönert [f], M. Shirchenko [l,d], H. Simgen [f], A. Smolnikov [d,j], L. Stanco [o], F. Stelzer [m], M. Tarka [q], A.V. Tikhomirov [l], C.A. Ur [o], A.A. Vasenko [k], A. Vauth [m], O. Volynets [m], M. Weber [f], M. Wojcik [b], E. Yanovich [j], S.V. Zhukov [l], D. Zinatulina [d], F. Zocca [i], K. Zuber [c], G. Zuzel [b],

[a]) INFN Laboratori Nazionali del Gran Sasso, LNGS, Assergi, Italy

[b]) Institute of Physics, Jagellonian University, Cracow, Poland

[c]) Institut für Kern- und Teilchenphysik, Technische Universität Dresden, Dresden, Germany

[d]) Joint Institute for Nuclear Research, Dubna, Russia

[e]) Institute for Reference Materials and Measurements, Geel, Belgium

[f]) Max Planck Institut für Kernphysik, Heidelberg, Germany

[g]) Dipartimento di Fisica, Università Milano Bicocca, Milano, Italy

[h]) INFN Milano Bicocca, Milano, Italy

[i]) Dipartimento di Fisica, Università degli Studi di Milano e INFN Milano, Milano, Italy

[j]) Institute for Nuclear Research of the Russian Academy of Sciences, Moscow, Russia

[k]) Institute for Theoretical and Experimental Physics, Moscow, Russia

[l]) Russian Research Center Kurchatov Institute, Moscow, Russia

[m]) Max-Planck-Institut für Physik, München, Germany

[n]) Dipartimento di Fisica dell'Università di Padova, Padova, Italy

[o]) INFN Padova, Padova, Italy

[p]) Physikalisches Institut, Eberhard Karls Universität Tübingen, Tübingen, Germany

[q]) Physik Institut der Universität Zürich, Zürich, Switzerland

Spokesperson: S. Schönert (*Stefan.Schoenert@mpi-hd.mpg.de*)

Deputy Spokesperson: C. Cattadori (*Carla.Cattadori@lngs.infn.it*)

Technical Coordinator: K.T. Knoepfle (*Karl-Tasso.Knoepfle@mpi-hd.mpg.de*)

URL: `http://www.mpi-hd.mpg.de/GERDA/`

Contents

1 Cryogenic vessel and infrastructure

Between September 30 and December 17, 2010, requirements and procedures for the cool down and filling of the GERDA cryostat were defined and examined in a series of five meetings between the LNGS director, SPP, Technical Division, Environmental Service and GERDA representatives. In addition to a final test of the GERDA safety and control system and its integration into the LNGS safety and control system, safety requirements included the installation of a water line of enhanced flow rate ($> 10\ell/\mathrm{s}$) to the exhaust gas heater, and the finalization of the GERDA ventilation line. It was decided that cool down and filling would be done with the water tank kept empty and by using exclusively the permanently installed GERDA cryogenic infrastructure, i.e. that the cold gas and LAr would be taken from the dedicated 6.3 m^3 LAr storage tank which in turn would be filled in the standard procedure by a tanker of the LAr supply company.

Green light for cool down was given for November 3, and the operation started one day later. With two shifts per day and a cool down rate that aimed at temperature gradients of less than 20 °C per hour and less than 50 °C across the cryostat, the operation was finished on November 9 (see Fig. 1) when first liquid argon was detected at the bottom

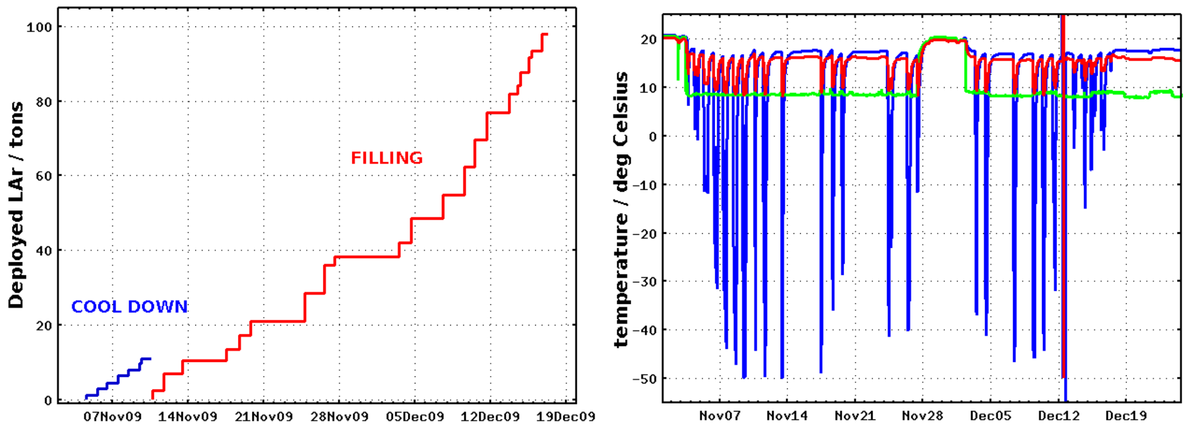

Figure 1: Left: History of the amount of liquid argon deployed during the cool down (blue curve) and filling (red curve) of the GERDA cryostat. Right: The temperature of the argon exhaust gas before (blue curve) and after (red curve) the exhaust gas heater during the cool down and filling phase. The 'heating' water temperature is indicated in green. Between November 27 and December 3 the flow of heating water was interrupted because of the installation of a new water line which increased the water flow rate from 4 to more than $10\,\ell/\mathrm{s}$.

of the cryostat. A total of less than 10 tons of LAr was deployed; the typical exhaust gas rate was about 150 m^3/h. In view of the very smooth cool down operation filling started immediately on November 10 and continued without any critical event until December 17 when the cryostat was filled up to the neck. A few intermediate stops (see Fig. 1) were scheduled for convenient LAr supply or refurbishment of the water supply for the exhaust gas heater. Filling was done with about 3 bar pressure at the storage tank's exit port while operating the cryostat at an absolute pressure of 1.2 bar in order to keep flash gas losses between 1 to 5 m^3/h; the filling rate of typically 0.7 m^3/h was thereby limited by the very fine filter in the LAr fill line.

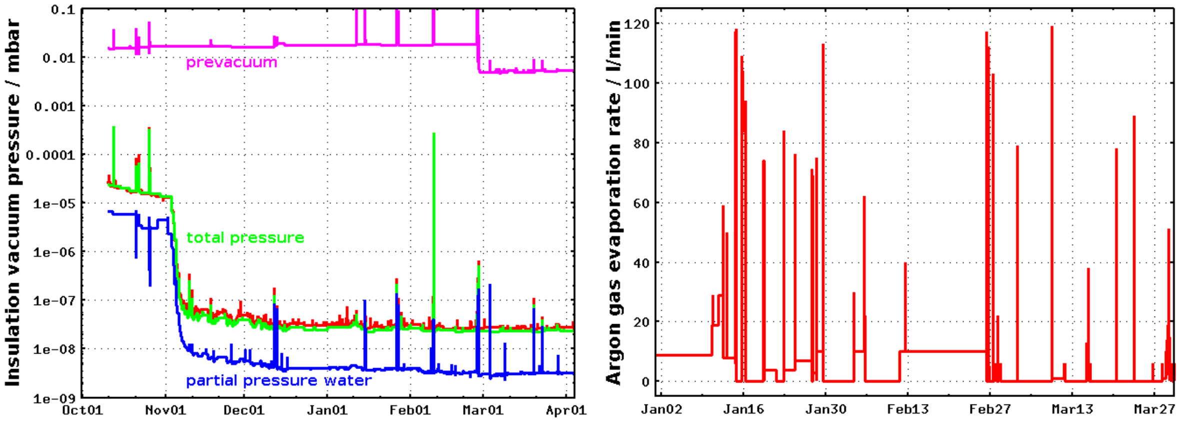

Figure 2: Left: History of insulation vacuum pressure in 2009/10. The improvement of the prevacuum at the end of February is due to an exchange of the fore-pump. The total pressure (green and red curves) has been measured redundantly with two pressure gauges. Right: Argon gas evaporation rate in standard liter per minute proving the active cooling to work since the beginning of 2010. Spikes in the plots are mostly due to intended tests or stops of the PLC system during maintenance.

Figs. 1 (right) and 2 (left) illustrate the functioning of the exhaust gas heater during the cool down and filling phase and the history of the cryostat's insulation vacuum. The total vacuum pressure of about 10^{-5} mbar decreased during cool down by more than two orders of magnitude to values approaching $2{\cdot}10^{-8}$ mbar. The permanently installed residual gas analyzer shows that the predominant partial pressure is now due to water. The present outgasing rate is about $4{\cdot}10^{-7}$ mbar$\cdot\ell$/s and pumping of the insulation vacuum is still continuing. These figures prove also that both the various components of the cryogenic system and its programmable logic controller (PLC) show stable and safe performance since months. In fact, performance and safety status of the GERDA cryogenic vessel can be examined worldwide at any time via a web interface [1]; by example, Fig. 3 shows the safety summary web page.

The commissioning of the cryostat's active cooling system started still during the Christmas break taking advantage of the control features integrated in the web interface. The system is based on two heat exchangers which are located in the neck and in the top part of the main cryostat volume, respectively, and which can be cooled independently with an adjustable flow and mixture of cold nitrogen gas and liquid. As shown in Fig. 2 (right), the argon gas evaporation rate is essentially zero since the beginning of 2010 - the period

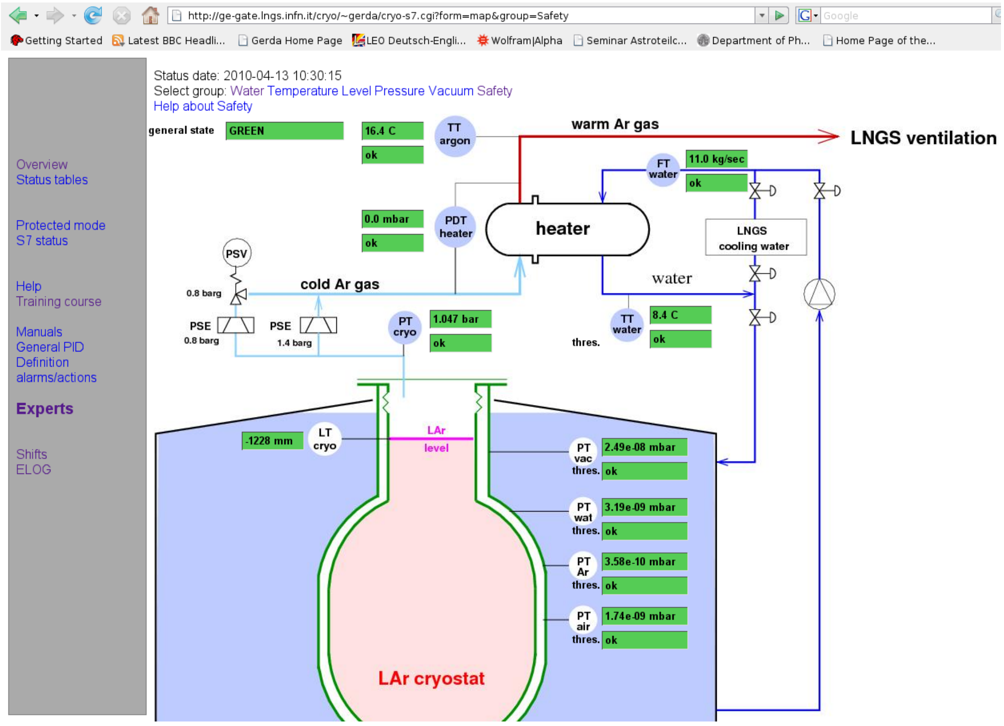

Figure 3: Safety summary web page of the GERDA cryogenic infrastructure.

with the small evaporation rate of about 10 ℓ/min in February was due to an unfavorable threshold setting in the monitoring routine and to a problem with the supply of liquid nitrogen. In fact, since the commissioning of the active cooling system the cryostat is exhibiting a practically constant LAr level eliminating virtually the need for LAr refills.

The commissioning of the active cooling system concluded the commissioning of the GERDA cryostat which is ready for use by the collaboration since January 2010. The transition from commissioning to routine operation became manifest also in the establishment of routine 24-hour safety shifts which are covered by both LNGS and GERDA members. The procedures for these every day shifts have been worked out together with the LNGS director and SPP. Safety shift documentation, the sign-on for shifts as well as present and past shift schedules are accessible via a dedicated web page. A training course for safety shifters following the March collaboration meeting has attracted more than 20 GERDA collaborators so that the load by safety shift duties is expected to move increasingly from LNGS to GERDA personnel, as requested by LNGS.

Permanent filling of the water tank is still awaiting the green light - for details see section 3. In the context of the cryogenic safety system it is here important to note that LNGS and GERDA have agreed to trigger in case of emergency[1] the water drainage automatically by the GERDA PLC (manual operation of the respective valves remains still

[1]For definition of GERDA alarm levels and corresponding actions, see ref. [2].

possible as a backup). The updated GERDA piping and instrumentation diagram [3] shows also that in the emergency case, water from the water tank can be used as 'heating' water for the exhaust gas heater being subsequently pumped at 20 ℓ/s to two of the three former GNO pits (or back to the water tank). This and the results of various water drainage tests have led to agree on a total water drainage rate of 117 ℓ/s in case of emergency. Compared to earlier specifications, this rate has almost doubled. It will have no or only minor impact on other activities in the underground laboratory allowing nevertheless to empty the water tank completely in less then the targeted 2 hours.

2 Clean room and lock systems

2.1 Clean room infrastructure

Since the last report to the scientific committee the works on the gas and vacuum systems have been started. The installation is to be finished until Mid April.

2.2 Commissioning lock

After the tests in Hall di Montaggio last year [4] the glove box has been transferred from hall di Montaggio to the clean room underground in November 2009.

Figure 4: Commissioning lock being tested on a hoist. The string was lowered to its design position fifteen times. The commissioning lock plus the attached white tube were flushed with dry nitrogen. Within the tube class 10.000 clean room conditions were assured before the tests.

Several mechanical improvements of the commissioning lock system were suggested. They included a mechanical stabilization of the linear pulley guide system, a friction clutch limiting the force on the steel rope, the installation of a *meter drive* measuring the real position of the string, installation of inductive sensors that serve as end switches as well as an additional camera that monitors the horizontal arm. The first cable arm has been assembled in the MPI Munich clean room surrounding implementing all suggested improvements. The system has been fully mechanically tested. It has been repeatedly released (15 times) to its design position with a dummy weight attached. The test has been performed in clean surrounding in the form of a tube that has been constantly flushed with dry nitrogen. Before the tests the clean room class had been established to be 10.000 or better (see Fig. 4).

The cable arm has been delivered to LNGS on 25 March 2010. It has been transferred to the clean room and installed onto the glove box. The PLC system has been installed and is available for use.

In order to deploy all available enriched germanium diodes it is necessary to modify the second cable arm. The vertical part of the lock system has to be enlarged. The string has to be modified such that up to nine detectors can be safely deployed. A first mock up of the system has been tested at MPI-K in Heidelberg (see Fig. 5). The design of the linear pulley system needs slight modification due to the extra weight. It is based on the first cable arm already delivered to LNGS. The winding mechanism and the cable chain have to be modified. Construction of the second cable arm starts in April 2010. Delivery to LNGS is expected for mid 2010.

Figure 5: Mock up of the cable arm holding three strings with three detectors each.

2.3 Final lock

The pressure and vacuum tight cylinder for the final lock system capable of deploying up to 80 detectors has been constructed and approved by the TÜV according to the pressure vessel code AD2000 (see Fig.6). Installation works on the final lock system will start as soon as the second cable arm of the commissioning lock system has been delivered to LNGS.

Figure 6: Inner and outer lock cylinders with both cable arms mounted.

3 Water tank drainage

Green light for the permanent filling of the water tank is expected soon when the final hardware for the drainage of the water tank is installed. Since September 2009, monthly meetings with the LNGS director, SPP and GERDA representatives and several tests have led to an improved configuration for the fast drainage of the water tank as compared to the earlier 'Carelli' proposition. In this document it was foreseen to drain the water tank through the new 250 mm diameter pipe below the TIR tunnel at 46 ℓ/s, and via the grid to one of the former GNO pits at 17 ℓ/s. Since these flow rates do not allow to empty the water tank (600 m^3) within the projected 2 hours completely, it was suggested for the case of maximum emergency to open one of the water tank's DN300 flanges and flood the hall A and the TIR tunnel. The GERDA collaboration has decided not to implement this latter option for two reasons: (1) its detrimental aspects outweigh the benefits: while still not allowing the 'immediate' drainage, the anticipated damage to nearby persons and experiments in case of false alarm seemed unacceptable, and (2) various drainage tests have proven that the new pipe in the TIR tunnel allows to drain water[2] at 80 ℓ/s, almost twice as much as assumed in the Carelli report, without affecting personnel or other installations in the underground laboratory. In addition, with two further drainage lines to two former GNO pits (100 m^3 each) - via the grid around the water tank at up to 17 ℓ/s and via a

[2]For routine drainage the flow rate shall be kept below 20 ℓ/s.

dedicated pump at 20 ℓ/s - the total drainage rate approaches 117ℓ/s which is enough to empty the water tank within 2 hours completely.

The prerequisite for this performance is the adherence to the respective flow rates which is trivial for the pumped line but more difficult for the two other lines where - without regulation - the flow rate decreases with decreasing water level. In fact, several test showed that the available as well as the refurbished passive regulators failed, presumably to the insufficient pressure drop. This problem has found an elegant solution in the context of the further decision that the condition for emergency drainage will be evaluated by the programmable logic controller (PLC) of the cryogenic infrastructure. This PLC will not only automatically trigger the actuators for opening the valves of the water tank but it will also maximize the flow rate in the main line up to 80 ℓ/s by opening a butterfly valve according to the decreasing water level. The major hardware components for this system are available and its installation will be concluded in a few weeks.

4 The Muon Veto

The installation of the muon veto [5] has been accomplished during the year 2009. Some external components like the splitter-box and the LED driven pulser system are being worked on. The data acquisition (DAQ) system has been installed in Tübingen and tested there with a smaller test tank equipped with 9/11 PMTs in order to adapt the software.

During this March, a test of the DAQ system and photo multiplier tubes (PMTs) of the GERDA muon veto has been performed, even with the water tank only about half full. Two PMTs at the bottom of the water tank showed unsuitable signals which will be repaired or exchanged before the water tank is finally filled. All other 64 PMTs showed normal signals. Light produced via the diffuser balls could be seen also by PMTs mounted on the opposite side of the water tank, i.e. whose direct sight was obstructed by the cryostat. Data sets were taken with the different light source on, but also with muon triggers. Two examples of the latter are shown in Fig. 7. The traces of the 9 and 13 PMTs having fired, respectively, are shown. While the event with 9 PMTs (right side) is clean without after-pulses, the other event on the left seems to be more violent with close-by secondaries within the next 1 μs. Reflections should have died out within less than 100 ns.

Presently, more software for analysis and monitoring is being developed. The software will comply with the standards discussed and set by the task groups 10 and 13 (see sec. 10,11).

A final test of all PMTs will be performed when the water tank is completely full, i.e. when all PMTs are immersed under water.

After 4 years in water under a pressure of about 1.1 bar, a test capsule had been opened and was investigated. After removal of the oil and the PMT, the steel capsule has been cut open and the bottom part has been cut in half as shown in Fig. 8. Details of the blue socket, capacitor and resistors can be recognized. This was to prove that the PU filling around the base was still intact. Actually, the surface was concave and showed no sign of swelling or deformation. A possible reaction of the oil with the PU can be excluded.

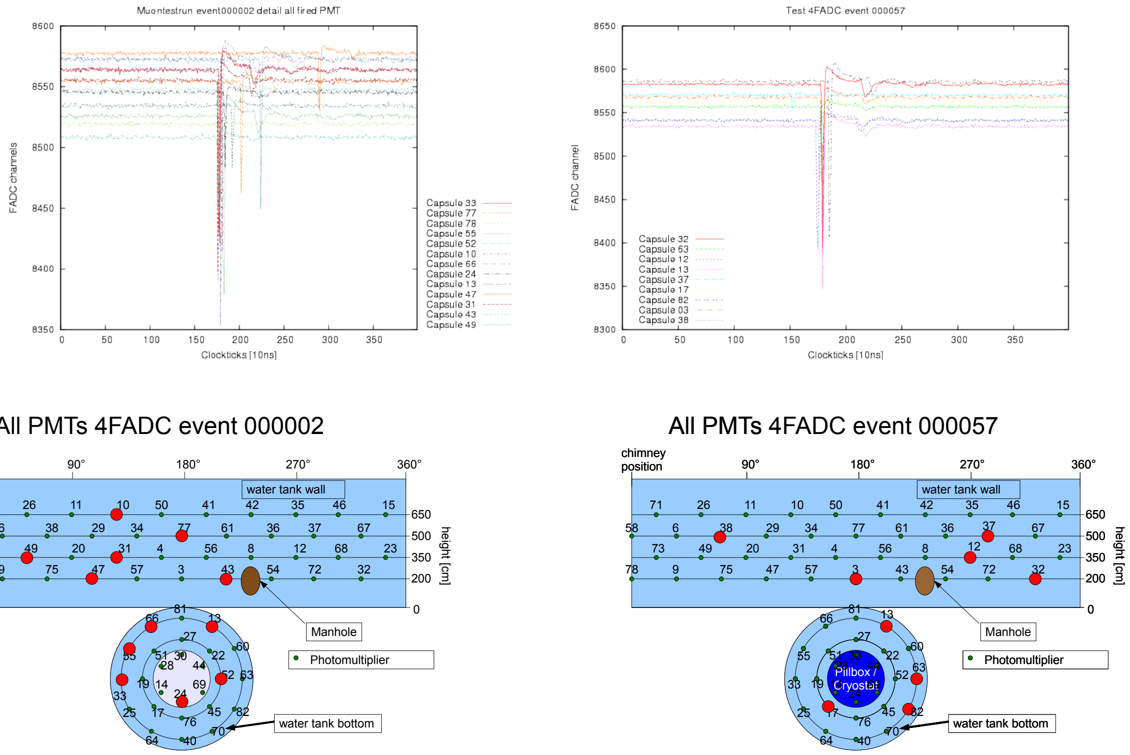

Figure 7: Two muon events in the water tank. The top row shows the traces in the relevant PMTs where one clock tick correspond to 10 ns. The bottom row demonstrates the two hit patterns by showing the fired PMTs by red dots in the map of the water tank.

Figure 8: Cross section of the socket of a test capsule which had been stored for 4 years in a test tank under water with overpressure.

5 Phase I detectors and R&D for liquid argon instrumentation

After the successful completion of the integration test in hall di montaggio, summarized in the last progress report, the activities of task group one (TG-1) focused *i*) on the preparation of the non-enriched detectors (work package 4+, WP4+) and their integration into a 3-detector string to be deployed in the commissioning lock, *ii*) on the tests of a bare BEGe detector operated in liquid argon reported in Sec. 9, and *iii*) on the commissioning and start-up of the GERDA low-background test-stand LArGe in the GDL (WP5).

5.1 Detectors for phase I start-up

After completion of the installations of the commissioning lock in the clean room, expected in CW 18, and the deployment of a mock-up detector for mechanical and electronic tests, a single non-enriched detector ('prototype detector') will be deployed in the liquid argon tank. The purpose is to test and debug the spectroscopic performance of the full system, similarly as it was done in the hall di montaggio integration test. Subsequently, a string with three non-enriched GTF-detectors, or alternatively with two non-enriched GTF-detectors and one enriched detector, will be mounted in one string and deployed. It is planned to operate the string with the three detectors for about two months in the GERDA cryostat in order to measure the background of the full detector assembly in the GERDA setup. Subsequently, it is planned to start the deployment of the enriched phase I detectors.

The detectors GTF32 (mass: 2321 g), GTF45 (2334 g) and GTF112 (2967 g) have been mounted in their low-mass holder and tested in liquid argon in Test Bench-1 in the GERDA underground Detector Laboratory (GDL). With the front-end electronics of this setup (60 cm cable between detector and FET operated in cold argon gas; FET separated from discrete preamplifier), the achieved energy resolutions are 2.5 keV full width at half maximum (FWHM) at 1.3 MeV for GTF32, 2.6 keV for GTF45 and 2.5 keV for GTF112. All leakage currents were stable at a few tens of pA and the detector assemblies are ready for deployment in the GERDA cryostat as soon as the commissioning lock installations are completed.

5.2 Low-background test stand LArGe

The first liquid argon filling of the GERDA low-background test stand LArGe, located in the GDL, was carried out in November 2009. The cryogenic commissioning was successful. The argon is subcooled to -187 ^{o}C with a liquid nitrogen flow into the heat exchanger of 2.05 m^3 (STP) per hour. The pressure is adjusted to about 960 mbar absolute by fine tuning of the active cooling setting. No argon is lost by evaporation under this operational condition.

After starting up the photomultipliers, it turned out that the scintillation light was quenched and the triplet life-time quasi invisible. It could be verified that the quenching was related to a contamination of the liquid argon which most likely was introduced into the setup through a leak after filling. The cryostat was emptied and warmed up over Christmas, and the leak fixed. The improvement and stability of the gas quality was monitored throughout the pumping and argon gas flushing cycles using mass spectrometry and by measuring the triplet life time of the argon gas scintillation in response to an internal alpha source. The second liquid argon fill was carried out in February. So far, the scintillation triplet life time is stable within the experimental uncertainties of 820 ± 40 nsec displayed in Fig. 9, similar to that measured in mini-LArGe with the same liquid argon quality.

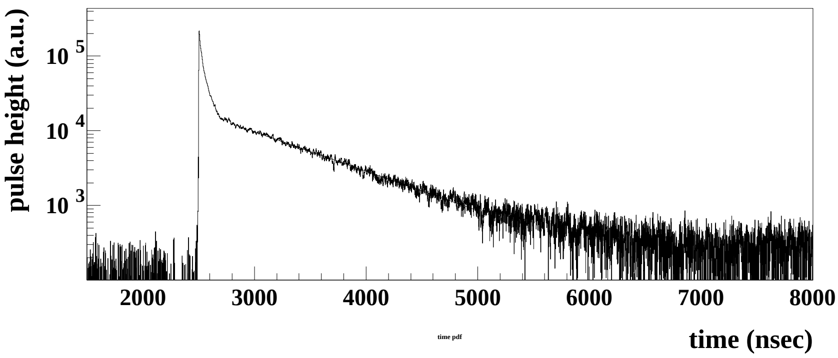

Figure 9: Averaged oscilloscope pulses from liquid argon scintillation in LArGe in response to an external ^{228}Th gamma source. The fast singlet and slow triplet component of the scintillation signal are clearly visible.

A preliminary analysis of the normalized photo-electron (pe) yield corresponds to 100 to 200 pe/MeV without significant position dependence. It is by a factor 5 to 10 reduced with respect to the values measured in the mini-LArGe setup. The light yield is however sufficient to operate the setup in the planned anti-coincidence mode. With a single photo electron (spe) trigger rate of approximately 20 kHz, and an anti-coincidence time window with the germanium signal of 1 μs, the accidental veto rate would correspond to about 2%, for an spe-signal as anti-coincidence condition. The corresponding threshold for energy depositions in liquid argon is approximately 10 keV. The accidentals are fully negligible at higher spe-multiplicities. Investigations of the origin of the reduced pe-yield are under preparation.

6 Status of Front End Electronics

In the last semester the activity focused on the following items:

6.1 Three channel circuit using PZ0

Three PCBs fully populated with

- the three channel PZ0 ASIC chip bonded on board and with a Cu protecting cover,
- all physical devices (front-end FET, R, C etc),
- the pins to connect all PCB input/output cables

have been individually measured at the γ-ray spectrometer. The 3 individual measurements are statistically compatible, indicating that the production procedure is reproduceable. The averages are reported in table 1. The overall ^{228}Th concentration of $\sim$350 μBq

	^{238}U/^{226}Ra [mBq/PCB]	^{232}Th/^{228}Ra [mBq/PCB]	^{232}Th/^{228}Th [mBq/PCB]	^{40}K [mBq/PCB]	^{210}Pb [mBq/PCB]
PCB	0.54 ± 0.08	0.24 ± 0.09	0.29 ± 0.08	3.2 ± 0.8	$< 5.3 \cdot 10^3$
22 pins	< 0.08	< 0.14	0.06 ± 0.2	0.44 ± 0.22	

Table 1: Radionuclides concentration in the fully populated PZ0 circuits and pins for the input connectors.

has to be compared to the value of 500 μBq which corresponds to a background index of 10^{-3} cts/(keV·kg·y) for the top detector for the planned PCB separation of $\sim$40 cm. Moreover 8 new PCBs made from cuflon have been produced with the qualified technology. Glueing and bonding of the PZ0, sealing with the Cu cup and populating the PCB with the selected solder paste is ongoing. Therefore 33 channels will be available for Phase I. The activity on the γ-ray screening of physical components to be used in the PCB production is continuously ongoing.

6.2 Charge sensitive amplifier based on commercial OpAmp

Since the second semester of 2009, we started to develop a Charge Sensitive Amplifier (CSA) based on commercial CMOS OpAmp devices that recently appeared on the market and which perform adequately for low-noise applications in a wide range of temperatures from room temperature down to cryogenic ones. The CSA architecture is the same as for the one based on the PZ0 CMOS ASIC, i.e. the front end Philips BF862 JFET is followed by the commercial OpAmp and discrete feed-back components.
After testing the PCB called CC2 at room and at liquid nitrogen temperature, it was connected to our encapsulated SUB detector and operated for 2 weeks. We achieved the following performances:

- Intrinsic energy resolution 0.7 keV for C_{det}=0 pF, with a slope of 16 eV/pF,
- sensitivity 100 mV / MeV for germanium,
- 30 ns intrinsic rise time,
- stable operation with a reduced number of passive components (filtering capacitors),
- cross-talk among the 3 channels $< 0.1\%$ when one output drives 50 Ω load,
- dissipated power < 50 mW/channel.

Beside these features the CSA is very reliable also for mechanic aspects: there is no need for a Cu cup to protect bonds, very simple and low-cost even in its low-radioactivity version.
A low radioactivity CSA (8 PCBs with 3 channels each) is under production made from cuflon and processed with the already qualified procedure using the same physical components as selected for the PZ0 based CSA. A major improvement has been the substitution of the feed-back and test capacitors ($\sim$ 1 pF) with printed-on-board ones as shown in Fig. 10. We expect at total activity of less than 100 μBq for ^{228}Th.

6.3 PZ1: Upgrade of PZ0 ASIC

The upgraded ASIC PZ1 chip has been produced at the foundry at the end of last year and is at present under test. It behaves as well as the PZ0 in terms of noise and it drives 50 Ω load. The test of running it with a detector will be done in the next future.

7 DAQ electronics and online software

7.1 DAQ system for the Ge detectors

The DAQ system for the Ge detectors was modified to make it more stable and reliable. We developed a new firmware for the FPGA controlling the transfer of the digitized data and corrected some bugs that manifested while testing the previous versions. The new version is controlling and maintaining the synchronized DMA transfer of the data when more than one PCI board is used by implementing a Master-Slave relationship among the boards. One of the boards is identified as Master and it waits the confirmation from all the other boards that the data transfer is finished before issuing the readout interrupt. This is an important feature of the system as we do not have control on the data transfer when DMA is enabled and one has to be sure that all data were already transferred from the PCI boards to RAM before starting the readout. The final system is running with the PCI boards at 32 bit/33 MHz and we verified that we can reach the maximum transfer rate of 132 MB/s. The data transfer to disk is limited by the present hard drives. With an upgraded system mounting SATA II hard disks we reached up to 60 MB/s transfer rate.

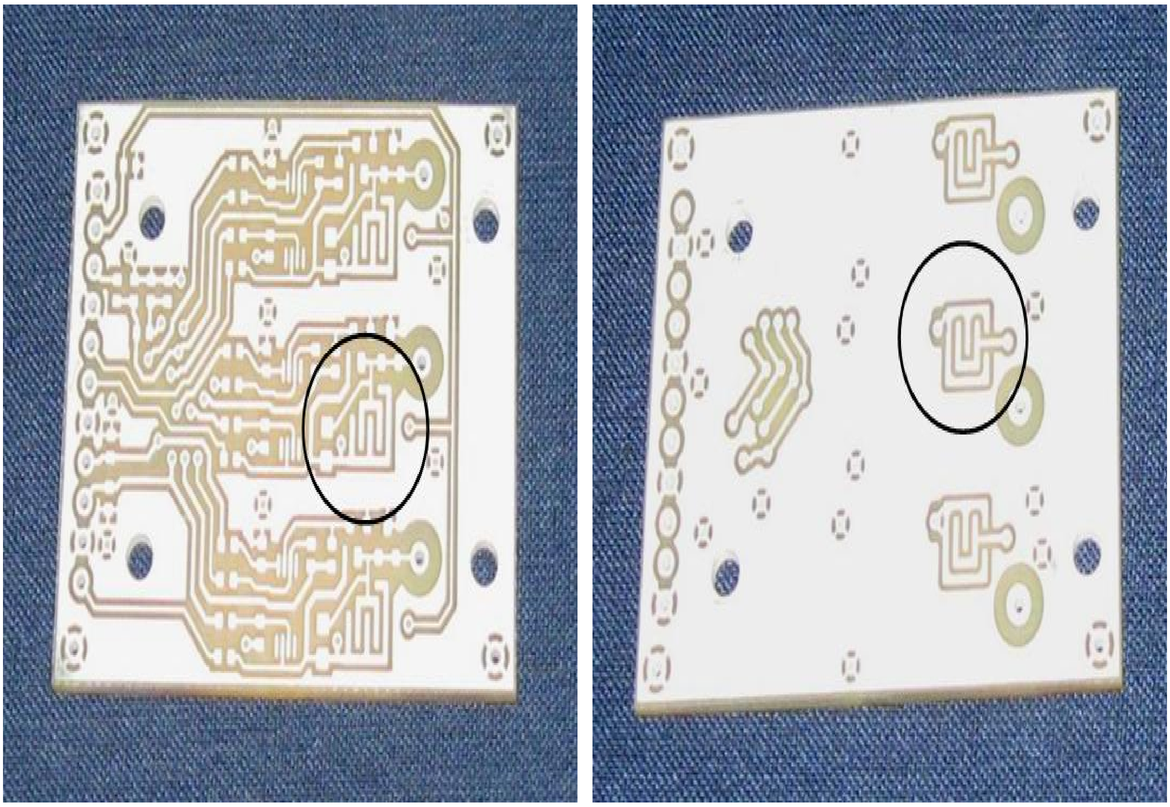

Figure 10: The new CC2 PCB with test pulse and feed-back capacitors printed on board: left is top side, right is bottom side.

For 10 channels this corresponds to a 2 kHz event rate. The system is presently installed in the gallery at its final position in the electronics cabinet and extensive operation tests are ongoing. A picture of the system located in the electronics cabinet is shown in Fig. 11 (left).

Another feature implemented is the possibility of producing the trigger internally for each channel separately. We have produced the firmware for programming the FPGA's mounted on the NIM boards to produce a TTL logical trigger signal that can be used for constructing the global trigger signal. The thresholds are programmable through a serial interface. We have performed tests of the trigger system under ideal conditions by using a pulser that produces signals with similar characteristics as the Ge detectors and we have obtained a threshold as low as 0.75 mV for full input range of 2 V. The same FPGA producing the trigger signals is used to monitor baseline shifts of the Ge diodes to identify changes in the leakage current. Integration with the Slow Control for issuing alarms and actions is under way.

We performed a test of the system with a BEGe detector and we found optimal performances close to the analogue electronics energy resolution and a trigger threshold of about 10 keV for a full range of about 6.6 MeV. The recorded spectrum is shown in Fig. 12.

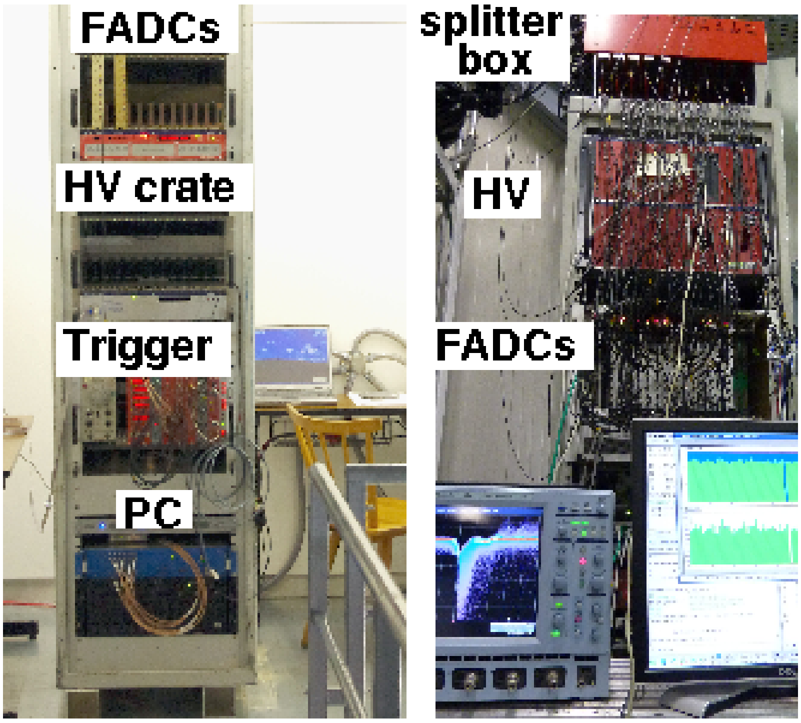

Figure 11: Left: The Ge DAQ system installed in the third floor electronics cabinet. Right: The muon veto DAQ installed in the second floor.

7.2 Muon veto DAQ

Eight veto channels with individual triggers are integrated on a commercial VME card. In total 12 boards are available for the digitization of the analog PMT signals. Every VME card has one trigger output which is the “OR” of all channels. These signals are combined on another VME card with an FPGA for a coincidence trigger, time stamping of the events and other control functions needed e.g. for the synchronization of the veto with the germanium detector readout.

The veto can not only trigger by itself but accepts also triggers from the germanium readout and stores 40 μsec traces. Within this time window, muons can be identified by counting the number of PMT hits and also by the analog sum of PMT signals. This allows especially in the early phase of the experiment a more careful analysis of the likelihood of a muon candidate. The time difference between a muon and an event in a germanium diode can be measured with 10 nsec resolution. This analysis is performed offline.

Recently, all electronics was assembled in Hall A (see Fig. 11 right) and the PMTs and the readout were tested for the first time with a partially filled water tank (see section 4 for details). Still missing is the integration of the light calibration system into the DAQ program.

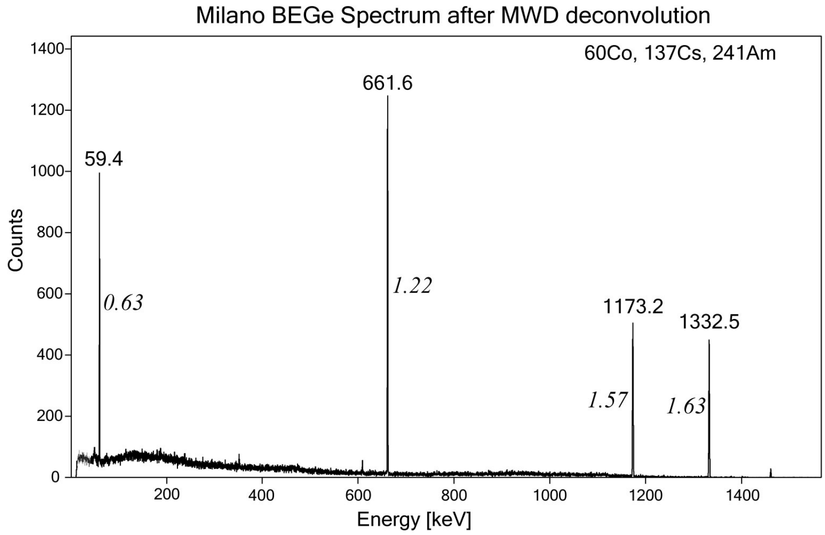

Figure 12: Gamma ray energy spectrum obtained by applying the MWD procedure to the waves recorded with the Ge DAQ system and the Milano BEGe detector. The energy of the γ-rays are written above the peaks while the corresponding FWHM are specified near the peaks with italic characters (all numbers in keV).

7.3 Slow Control and Network infrastructure

The main activities have been devoted to the following items:

1. completion of the computing network in Hall A;
2. building of the general structure of the Slow Control;
3. integration of the sub-components in the Slow Control framework.

The layout of the GERDA Network Structure and of its services were explained in detail in a previous progress report [11]. In the meantime the system has been implemented. Many computers and PLCs controlling the various sub-components are now connected.

The general structure of the Slow Control (see refs. [12, 13]) is almost ready. That is the central database was installed in the computer dedicated to the Slow Control and now it is collecting the data coming from the clients. The data stored in the data base can be accessed through a WEB server. The alarm generator and the alarm dispatcher have been developed and now they are in a debugging phase ready to be used by the components.

The integration of the various sub-components has started. At the time of writing all the sensors of the cryostat and of the clean room have been successfully integrated. In the following months the integration of the other sub-components will follow. A data sample from the database and an histogram of the values collected from a sensor of the cryostat are shown in Figs. 13 and 14, respectively.

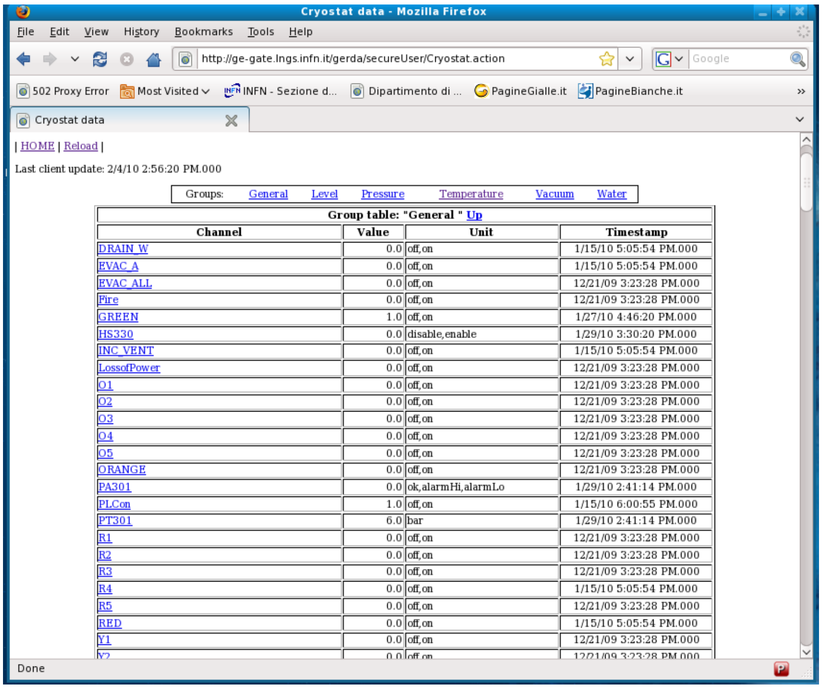

Cryostat data - Mozilla Firefox

http://ge-gate.lngs.infn.it/gerda/secureUser/Cryostat.action

| HOME | Reload |

Last client update: 2/4/10 2:56:20 PM.000

Groups: General Level Pressure Temperature Vacuum Water

Group table: "General " Up

Channel	Value	Unit	Timestamp
DRAIN_W	0.0	off,on	1/15/10 5:05:54 PM.000
EVAC_A	0.0	off,on	1/15/10 5:05:54 PM.000
EVAC_ALL	0.0	off,on	12/21/09 3:23:28 PM.000
Fire	0.0	off,on	12/21/09 3:23:28 PM.000
GREEN	1.0	off,on	1/27/10 4:46:20 PM.000
HS330	0.0	disable,enable	1/29/10 3:30:20 PM.000
INC_VENT	0.0	off,on	1/15/10 5:05:54 PM.000
LossofPower	0.0	off,on	12/21/09 3:23:28 PM.000
O1	0.0	off,on	12/21/09 3:23:28 PM.000
O2	0.0	off,on	12/21/09 3:23:28 PM.000
O3	0.0	off,on	12/21/09 3:23:28 PM.000
O4	0.0	off,on	12/21/09 3:23:28 PM.000
O5	0.0	off,on	12/21/09 3:23:28 PM.000
ORANGE	0.0	off,on	12/21/09 3:23:28 PM.000
PA301	0.0	ok,alarmHi,alarmLo	1/29/10 2:41:14 PM.000
PLCon	1.0	off,on	1/15/10 6:00:55 PM.000
PT301	6.0	bar	1/29/10 2:41:14 PM.000
R1	0.0	off,on	12/21/09 3:23:28 PM.000
R2	0.0	off,on	12/21/09 3:23:28 PM.000
R3	0.0	off,on	12/21/09 3:23:28 PM.000
R4	0.0	off,on	1/15/10 5:05:54 PM.000
R5	0.0	off,on	12/21/09 3:23:28 PM.000
RED	0.0	off,on	1/15/10 5:05:54 PM.000
Y1	0.0	off,on	12/21/09 3:23:28 PM.000
Y2	0.0	off,on	12/21/09 3:23:28 PM.000

Done

Figure 13: A snapshot of the data stored in the Slow Control database and coming from a part of the cryostat sensors.

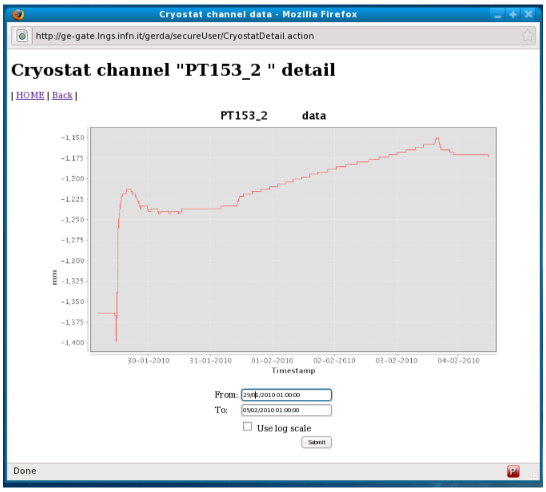

Figure 14: Histogram of the historical data from one cryostat sensor.

8 Calibration

8.1 Monte Carlo simulations

Since the last report, our Monte Carlo efforts were focused on simulating the gamma and neutron induced background from the calibration sources in their parking position for the final Phase I configuration. The geometry of the simulated Phase I detector array with the three calibration sources and their absorbers is shown schematically in Figure 15. For three ^{228}Th calibration sources, with an activity of 20 kBq each, we obtain a conservative background rate of $3{\times}10^{-5}$events/(kg y keV) and $2.4{\times}10^{-5}$events/(kg y keV) in the region of interest for the neutrinoless double beta decay from the gammas and neutrons emitted by these sources, respectively. We have also studied the background coming from neutron capture in detector and surrounding materials while the sources are in calibration and in parking position. Of all the produced isotopes, only ^{77}Ge is potentially dangerous. It decays with $T_{1/2}$ = 11.3 h, has a Q-value for the β-decay of 2.7 MeV and emitts several gammas with energies up to about 2.35 MeV. Assuming a neutron flux of $9{\times}10^{-4}$ n/(s kBq) (see Section 8.3), and a total activity of 60 kBq, we obtain a background rate of ($7.4{\times}10^{-6}$) events/(kg yr keV) in the signal region.

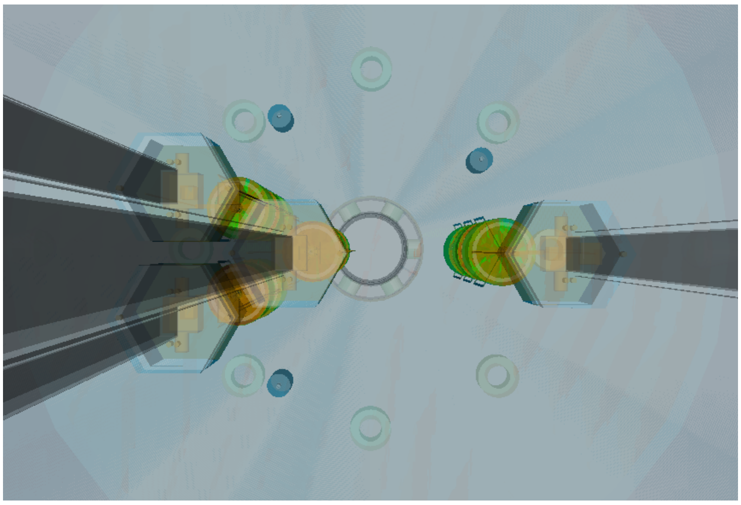

Figure 15: Top view of the Phase I detector array (four detector strings of three crystals each) with the three calibration sources along with their tantalum absorbers.

8.2 Source absorber, calibration and production of new sources

Three tantalum ring shields for the sources in their parking positions were mounted on the inside of the flange holding the sources. Subsequently, the lowering system for one of the calibration sources including the absorber was successfully tested on site. Several lowering cycles down to 10 m ensured that there are no oscillations of the system even with relatively high moving speeds and that there are no problems to insert the absorber into the tantalum ring when lifted. An upgrade of the currently manual lowering system to a motorized one is on its way. The tantalum rings and the aluminum pieces above the absorber have been screened with Gator, yielding the results shown in Table 2. Given the rather high ^{238}U, ^{235}U and ^{232}Th content of the aluminum holder, we have replaced it with a radiopure copper one.

Table 2: Results from the screening of the tantalum rings and the aluminum holders.

Material	^{226}**Ra** mBq/kg	^{238}**U** mBq/kg	^{232}**Th** mBq/kg	^{60}**Co** mBq/kg	^{40}**K** mBq/kg	**Others** mBq/kg
Aluminum holder	< 13	$(8 \pm 1) \times 10^3$	^{228}Ra 101 ± 25 ^{224}Ra 491 ± 56	< 5	< 65	310 ± 40 (^{235}U)
Tantalum ring	< 2.3	< 9.4	^{228}Ra < 2.2 ^{224}Ra < 3.2	< 0.5	< 3.88	21.3 ± 2.8 (^{182}Ta)

The custom made ^{228}Th source has been sent for a precise calibration to IRMM in Geel, along with a new, 25.5 kBq commercial source purchased from Eckert&Ziegler. Two new ^{228}Th custom sources have been produced: one of ∼30 kBq at PSI, and one of ∼40 kBq in Mainz. These sources have been sent for encapsulation to Eckert&Ziegler Braunschweig and will arrive at IRMM for a precise calibration by the end of April 2010. After the calibration procedure, the sources will be sent to LNGS where the neutron fluxes will be measured. To speed up this process, we are acquiring a LiI(Eu) neutron detector, will will be installed at LNGS in a few weeks. ^{6}Li has a large cross section for neutron capture (940 barns for thermal neutrons), the relevant reaction is n + ^{6}Li $\longrightarrow \alpha$ + ^{3}H + 4.8 MeV. The alpha and the tritium are stopped even in a thin layer of a LiI crystal and their full energy is detected. We are studying the optimal moderator thickness and shield configuration via MC simulations based on Geant4.

8.3 Neutron Flux Measurements and Predictions

We have remeasured the n-flux of the first custom source and of a commercial source from Eckert&Ziegler, with a ^{3}He counter at LNGS. The detector was inserted in a 6 cm diameter and 6 cm height polyethylene cylinder, which was wrapped in Cd foil and placed in a boron doped paraffin shield.

The neutron rates for the custom and commercial source were measured to be (2.7±0.5) $\times$ 10^{-2} n/s and (1.4±0.2) $\times 10^{-1}$ n/s, respectively. Considering that the sources had activities of 15 kBq and 43 kBq, we find a factor of about 1.7 difference in the n-rates. The ^{3}He counter was calibrated with an AmBe neutron source, with a flux of about (10±1) n/s, giving a neutron rate of about 0.72 n/s; hence above numbers assumed an efficiency of about 0.07 for both the AmBe and ^{228}Th sources. A Monte Carlo simulation of the actual geometry and the AmBe n-spectrum, as well as the ThO_2 n-spectrum yielded overall efficiencies

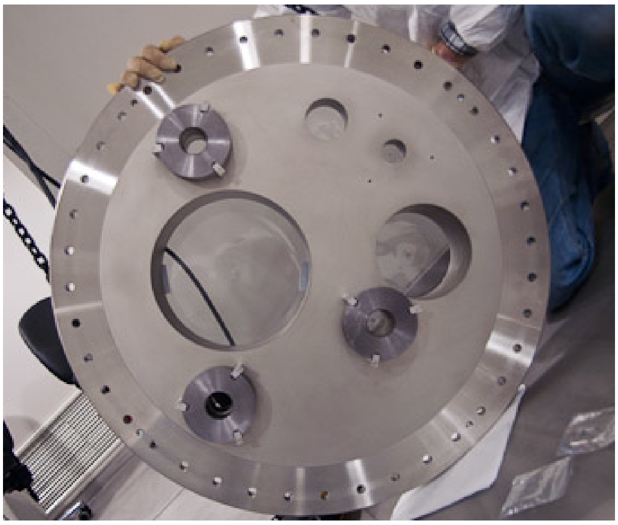

Figure 16: Calibration source flange with three tantalum rings mounted. The rings provide additional shielding against the gammas from the ^{228}Th sources in their parking positions.

of 0.095 and 0.152, respectively. Using these efficiencies, the neutron rate for the custom source goes down to about 0.013 n/s, or, using the activity of 15 kBq, to 9×10^{-4} n/(s kBq). These results will be cross checked by using the LiI(Eu) detector to be installed at LNGS. The relative gamma activities of the two sources have been determined with the Gator detector, by placing them on a thin stainless steel tube 10 cm above the detector's endcap.

We have cross checked our predictions of the neutron fluxes from the commercial and custom sources, and estimated the systematic uncertainties coming from the (α,n) cross sections. We have used the cross sections given in SOURCES, calculated the cross sections using EMPIRE, and also took measured cross sections from the EXFOR database. Since we find that there is quite some variation in the cross sections from these sources, in order to be conservative we have considered the upper and lower envelopes as a function of energy. We thus obtained following intervals for the neutron rates: [4.5–7.3]$\times10^{-4}$ n/(s kBq) for a $^{228}ThO_2$ source, [3.1–7.3] $\times10^{-2}$ n/(s kBq) for a ^{228}Th source embedded in $NaAlSiO_2$ and [2.1–4.2] $\times10^{-2}$ n/(s kBq) for a ^{228}Th source in Al_2O_3. We are also investigating potential contaminations in the custom $^{228}ThO_2$ source and their contributions to the measured neutron flux.

8.4 Analysis Pipeline of Calibration Runs

We have started to work on the analysis scheme of the calibration data. The raw calibration data will go through the same analysis pipeline as all other GERDA data. The basic event information (waveforms etc, called Tier-1) will be written out as MGDO objects. Subsequently, parameters such a energy, pulse rise-time, baseline noise, saturation etc (called Tier-2) will be extracted from the waveforms, using different reconstruction and noise-filtering algorithms. These algorithms, as well as the entire calibration analysis pipeline will be first tested on regular calibration data taken with a commercial ^{228}Th source and a natural HPGe detector at a local test facility. The goal of the calibration analysis pipeline is to calculate the position and energy resolution of the full energy peaks, as well as the number of events under each peak and to look at the stability of the calibration parameters with time. The calibration parameters for each detector and calibration run will be stored as MGDO objects, providing a direct interface with the Gerda analysis software. A web interface will also be provided, that will be used for the visual inspection of the individual detector spectra and parameters, and the evolution of these parameters in time.

9 Phase II Detectors

9.1 Purification of enriched Ge

After the terms of the contract were agreed we started the reduction and zone refinement of the enriched germanium at PPM Pure Metals, in Langelsheim. The 53.3 kg of enriched GeO_2 purchased from ECP in 2006 was stored until now underground at the SCK CEN Mol (HADES) underground laboratory in Belgium. On the 8th of March 2010 the boxes with the enriched GeO_2 were transported from HADES to the Rammelsberg mining museum in Goslar.

To minimize the exposure to cosmics during the production, the material is stored in an unused shaft of the old Rammelsberg mine. Only the material that is being processed is taken out each time before the production starts and taken back underground when it is over.

At the moment of writing 32.9 kg oxide was reduced to metallic germanium. The zone-refinement procedure starts each time when enough material is available to fill the boats. So far 7.7 kg of 6N material was produced but the production rate will increase as more metal is available.

The mean exposure after the first five reduction runs and of two zone-refinement runs is about 97.8 h slightly. This includes the 6 hour transport from HADES. The exposure is expected to increase as more zone-refinement runs will be necessary to achieve our goal of 90% yield of 6N material. Still, it will be much less than the original estimated total processing time of two month.

The zone-refinement is expected to end around 30th of April or soon after.

9.1.1 Crystal pulling

As reported earlier the major source of arsenic impurities in crystals pulled via the Czochralski technique at the Leibniz Institute for Kristallzüchtung (IKZ) was found to be the Czochralski puller itself. IKZ decided to dismantle the puller and send it to an external company for electro-polishing. Earlier this year the puller arrived back to IKZ and was reassembled. To date, two new crystals were pulled with this refurbished puller.

No significant arsenic contamination was found in the recently pulled crystals. So the cleaning procedure is considered to be a success. The net charge carrier concentration is about 10^{12} cm^{-3} with the dominant impurity being phosphorus. The next steps to reduce the phosphorus concentration are being discussed now. We are awaiting the results from the crystal grown from the clean parts of two previous crystals. It is believed that multiple crystal pulling will reduce the impurities considerably.

In the meantime, IKZ is working on an alternative solution for crystal pulling. They are modifying a float-zone puller to be used as a Czochralski puller. Using two different pullers they can exclude the possibility that the impurities come from the puller itself. The first crystal was already grown and results are expected soon.

All the crystals were analysed with photo-thermal ionization spectroscopy (PTIS) at IKZ and with photoluminescence (PL) in Dresden almost simultaneously and gave compatible results.

9.2 Development of 18-fold segmented n-type detectors

In the course of investigations of the 18-fold segmented prototype detectors several effects caused by the passivation and the (not) metalized surfaces could be observed. In order to better understand and to quantify these effects several special detectors were procured.

9.2.1 Detector with extra end-surface segment

In order to study surface effects of the passivation area an 18 + 1 segmented detector was procured and operated in a vacuum test cryostat. In addition to the three-fold segmentation in z and six fold segmentation in phi the detector had a 19th segment consisting of a 5mm thick disc below the passivation area, on one end of the crystal.

Scanning measurements of the segment showed that the dead layer beneath the passivation area is of the order of 1 mm. Several event types could be identified that are attributed to electron and hole trapping inside the detector [14].

9.2.2 Detector with special metalization

Previous prototype detectors were ordered with minimized metalization to reduce possible radioactive element deposition. In order to study effects due to the missing full metalization on individual segments a special detector was order and procured. It has 12 of the segments fully metalized and six of the segments metalized only around the contacting area (see Fig. 17). The detector has been operated in liquid nitrogen and data has been recorded. The data analysis is presently ongoing.

9.3 Pulse Shape Simulation for n-type segmented detectors

In order to improve the knowledge on background discrimination based on pulse shape analysis and potentially to improve its efficiency, a pulse shape simulation package has

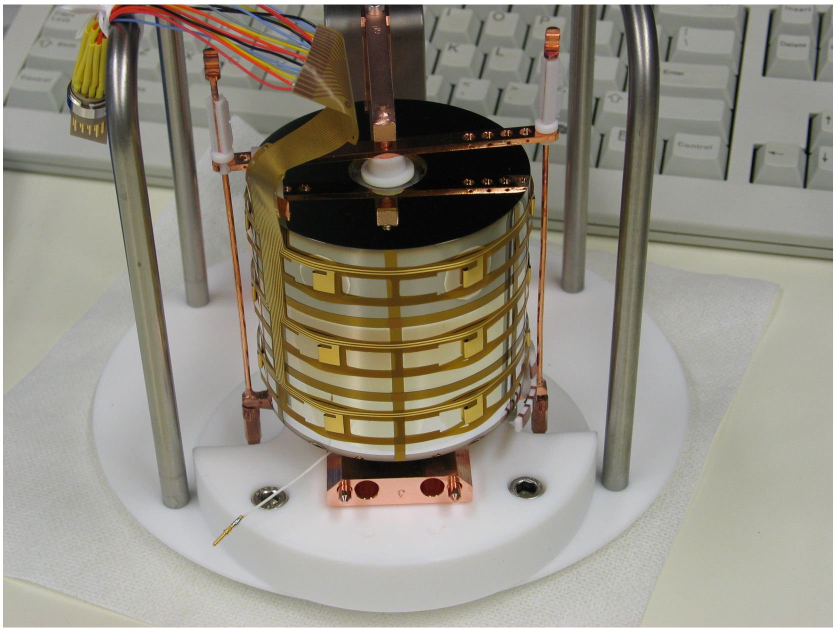

Figure 17: 18-fold segmented HPGe detector. The upper six segments are metalized only around the contact area. The segments in the middle and bottom layers are fully metalized.

been developed [15]. The package has been used to simulate pulses of one of the GERDA 18-fold segmented prototype detectors (see Fig. 18).

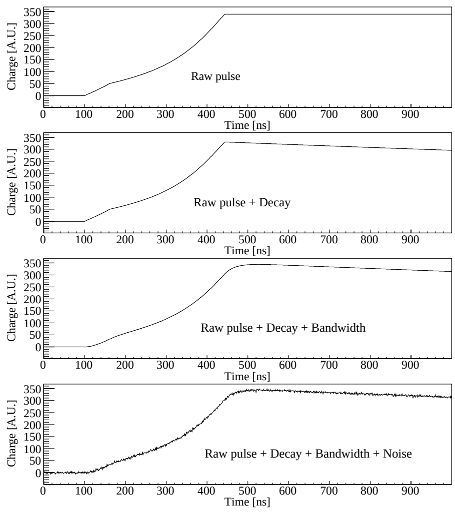

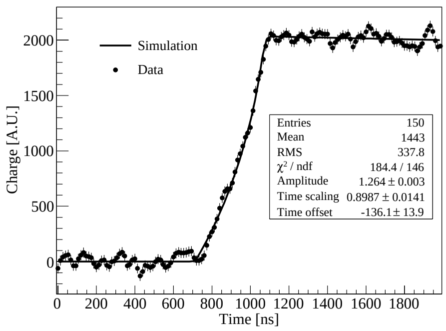

Figure 18: Left: Steps in simulating individual pulse shapes. Right: Direct comparison of an arbitrary data pulse with a simulated one.

The simulated pulses were compared to data taken with one of the GERDA prototype detectors. It could be shown that real pulses are well described by the simulated ones (see Fig. 18).

9.4 p-type BEGe detectors

During the last six months, the R&D for non-segmented p-type thick-window BEGe detectors for phase II focused on 1) the simulation of the characteristic signal pulse shape and discrimination (c.f. Sec. 10), 2) the performance of a bare BEGe detector in liquid argon, and 3) on the production and characterization of BEGe detectors from depleted germanium.

9.4.1 Detector performance in liquid argon

The 80 mm diameter BEGe detector was removed from its vacuum cryostat and operated as a bare detector in the liquid argon test bench in GDL. An energy resolution of 1.8 keV FWHM for the 1.3 MeV ^{60}Co line and a pulser resolution of 1.0 keV FWHM was achieved with about 35 cm cable length between crystal and FET. All detector parameters under observation (energy resolution, peak pulse height, count rates, leakage current, pulse shapes discrimination) were stable during a one month lasting stability test. The left part of Figure 19 displays the ^{228}Th spectrum prior and after pulse shape discrimination. Fixing the acceptance of the double escape peak to 0.9, the full energy peak at 1621 keV has a survival probability of 0.12 $\pm$ 0.02. Within the uncertainty, this value is identical to the one obtained with the same crystal operated in a vacuum cryostat. The right plot in Figure 19 shows the stability of the pulse shape analysis over time. For comparison the results achieved with the crystal mounted in the vacuum cryostat are displayed.

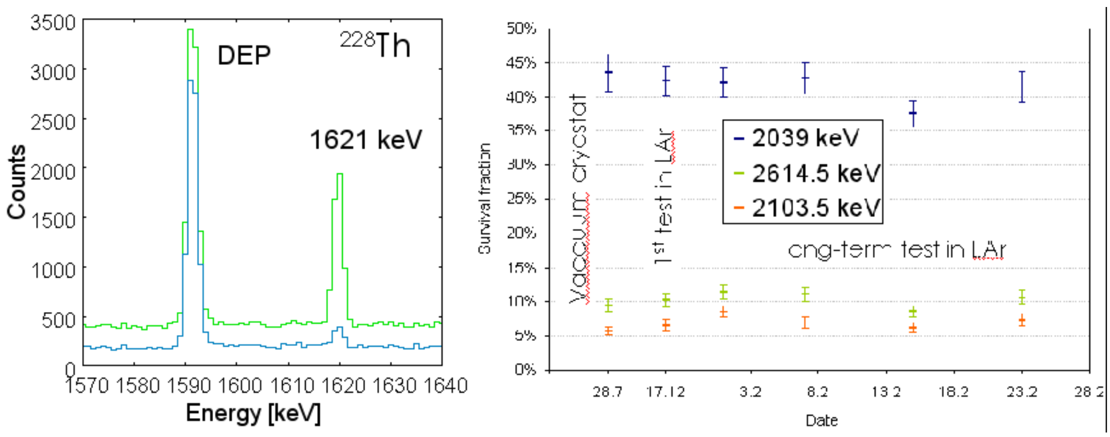

Figure 19: Discrimination of multi-site and single-site events by pulse shape discrimination with a bare BEGe detector operated in liquid argon. Left: Energy spectrum of double escape peak (DEP) and full energy peak (FE) peak at 1621 keV before (green) and after (blue) application of the pulse shape cut. Right: Long-term measurements to investigate the stability of the pulse shape cuts with time.

9.4.2 Thick-window BEGe detectors from depleted germanium

All four crystals were pulled by November 2009 according to specifications at the manufacturer in Oak Ridge with a total mass of 17.7 kg of depleted germanium. A first crystal cutting plan was worked out with the manufacturer following detailed field calculations and the first three detector slices arrived at the European detector manufacturer early January 2010. As the goal is to understand the maximum achievable detector yield, we decided to produce not only detectors from central parts of the crystals, but as well detectors from pieces close to the seed- and tail-end which usually are not used in the commercial detector production. A bevel type detector produced from the seed-end of crystal P81878, slice P81878AA, showed a increased leakage current which is presumably related to crystal defects close to the surface. The suspected part of the surface is currently being removed and a new detector will be produced from this slice for testing.

The other two detector slices, P81890CC and P81890DD, the latter a bevel type geometry from the tail end, were successfully transformed into detectors. The detectors mounted into standard cryostat passed the acceptance tests at the manufacturer and have arrived at LNGS on 29 March. First spectroscopic measurements showed an energy resolution of 1.62 and 1.67 keV FWHM at 1.3 MeV for the two detectors. The detailed characterization started on 6 April. First results on the pulse shape analysis based on the A/E ratio method are available for the bevel-shape BEGe detector (P8190DD): Fixing the acceptance of the double escape peak to $90 \pm 1\,\%$, the full energy peaks at 1621 keV and 2615 keV have survival probabilities of $11.3 \pm 0.6\,\%$ and $8.83 \pm 0.07\,\%$, respectively, the single escape peak of $5.8 \pm 0.4\,\%$, and the Compton continuum at $Q_{\beta\beta}$ of $39.8 \pm 0.3\,\%$. Within errors, the results are identical to those obtained with the cylindrical BEGe detectors of 80 mm and 70 mm diameter, and corroborate the simplicity and robustness of the detectors and of the analysis method.

The successful production of p-type BEGe detectors from depleted germanium material constitutes a major milestone towards the realization of the GERDA phase II detectors. It validated the production chain starting from isotopically modified raw germanium material from ECP, followed by chemical reduction and zone refinement at PPM Göttingen, crystal pulling at Canberra Oak Ridge, and detector fabrication at Canberra Olen.

We plan to produce two more detectors from different slices during the next months and study the expected mass yield of final detectors for the 37.5 kg of enriched material. The goal is to collect until summer the relevant information for the decision process which type of detectors to be produced from enriched germanium for phase II.

10 Simulations and background studies

In the last six months, the activity of the Task Group was mainly devoted to the definition and implementation of common analysis interfaces and algorithms, based on the MGDO software package.

Furthermore, the simulation activity of pulse shapes in the Ge detectors of interest for

GERDA went on, especially for BEGe's. This encompasses benchmarking and validation with experimental data.

10.1 Data objects and algorithms

A major activity within the Task Group was the continuous development, test and upgrade of the MGDO (Majorana-Gerda Data Object) software library, which is maintained jointly with the MAJORANA Monte Carlo group.

The MGDO libraries contain:

1. a set of generic interfaces and data objects to encapsulate, store and manage physical quantities of interest, as waveforms in time domain (`MGWaveform`), waveforms in frequency domain (`MGWaveforFT`), digitizer additional outputs (`MGVDigitizerData`), electric fields (`MGElectricField`), and geometry of detectors (`MGCrystalData`).

2. a collection of general-purpose tools ("Transforms") that operate on the waveform objects and can be used for actual data analysis. Tools available at the moment include filters (RC differentiator/integrator, trapezoid, moving average, etc.) and data handlers (smoothing, extremum finder, baseline removal, derivatives). New or alternative algorithms or analysis tools can be easily implemented through the general interface `MGVWaveformTransformer`.

3. ROOT wrappers for the data objects listed in the item 1 (e.g. `MGTWaveform` is the ROOT wrapper for `MGWaveform`). They make it possible to store the MGDO data objects (e.g. a `MGTWaveform`) within a ROOT `TTree` (= a n-tuple) or more generally in a ROOT format.

MGDO is a set of libraries, not providing any executable. Collaborators are hence supposed to write their own main program which relies on the MGDO format and tools.

Since the format of the raw data is dependent on the hardware configuration, it is advisable to convert raw data in a standardized format ("tier 1"), which is solid, flexible, exportable and easy readable by all collaborators. Also calibration and Monte Carlo data can be converted in the same format, allowing the analysis of Monte Carlo and calibration runs with the same algorithms and along the same analysis stream as real data. This is particularly important for the simulated pulse shapes. In this sense, MGDO containers represent a natural candidate for data storage in a unique format, as described in Sect. 11. The MAGE Monte Carlo framework is indeed able to produce simulated pulses in a MGDO-compliant output format.

A prototype analysis suite is currently being developed within the Task Group. It implements a modular analysis approach based on ROOT and TAM (Tree Analysis Modules) [6], which is able to read raw data from any source (real data, Monte Carlo, etc.) via the MGDO format. The suite is going to be tested, debugged and benchmarked in the measurement campaign with the ^{dep}Ge BEGe detectors at LNGS.

10.2 Simulation of background rejection performances of BEGe detectors

As described in the last report, a comprehensive simulation of the pulse signal formation and evolution was developed to study the performances and features of BEGe detectors [7]. In the last months the software was redesigned in order to better interface the pulse shape calculation to the Monte Carlo simulation and optimized to reduce the computation time. The conceptual flow of the simulation is now divided into two phases. As a first step, a library of pulses is created. The second phase includes the Monte Carlo simulation, followed by the pulse computation, which is performed as average of the pulses in the library. Therefore, the library must be generated only once for each experimental setup.

A software based on the MGS code [8] is used to create the library. The detector volume is divided in 1 mm-side cubic cells and for each vertex a pulse with a normalized amplitude is generated. Then all pulses are convolved with the response function of the DAQ and stored in a library.

The second phase starts with the MaGe Monte Carlo simulation, which provides for all events the position and the energy deposition of each hit. The pulse produced by each interaction site is computed from the reference pulses in the library, as weighted mean of the eight closest neighbors. The amplitude of the individual pulses is normalized according to the energy deposition and the total pulse of each event is obtained as a sum of the single interaction pulses. Noise is eventually superimposed to the event pulses. Noise is taken from a library of experimentally recorded baselines and its amplitude is normalized according to the experimental signal–to–noise ratio. By using the upgraded software, it is possible to generate a file of pulses completely equivalent of that of an FADC and apply the same analysis tools to both experimental and simulated data.

The first application of the simulation was the study of the Pulse Shape Discrimination (PSD) performances of BEGe detectors. The discrimination between single site events (SSE) and multi site events (MSE) can be done according to the ratio between the maximum amplitude of the differentiated signal and the energy loss in the detector [9, 10].

The main sources of background expected in the Gerda experiment can be divided into two categories: external and internal sources. The external sources of background, e.g. ^{232}Th and ^{60}Co, are due to the not perfect shielding from the natural radioactivity. The internal sources, i.e. ^{60}Co and ^{68}Ge, are due to the activation of Ge isotopes inside the detectors as a consequence of cosmic ray interactions.

To check the reliability of the simulation, the discrimination performances for experimental and simulated data obtained with external background sources have been compared. In particular, a BEGe detector was irradiated with ^{232}Th and ^{60}Co sources. The PSD results obtained with the calculated pulses show a good compatibility with the experimental results.

Then, the discrimination power for internal background sources was evaluated by means of the simulation. Figure 20 shows the spectra of internal ^{60}Co and ^{68}Ge before and after the PSD cuts described in Ref. [9]. The estimated survival probability in the $Q_{\beta\beta}$ region is 0.8% for ^{60}Co and 4% for ^{68}Ga (progeny of ^{68}Ge) when adjusting the acceptance of the

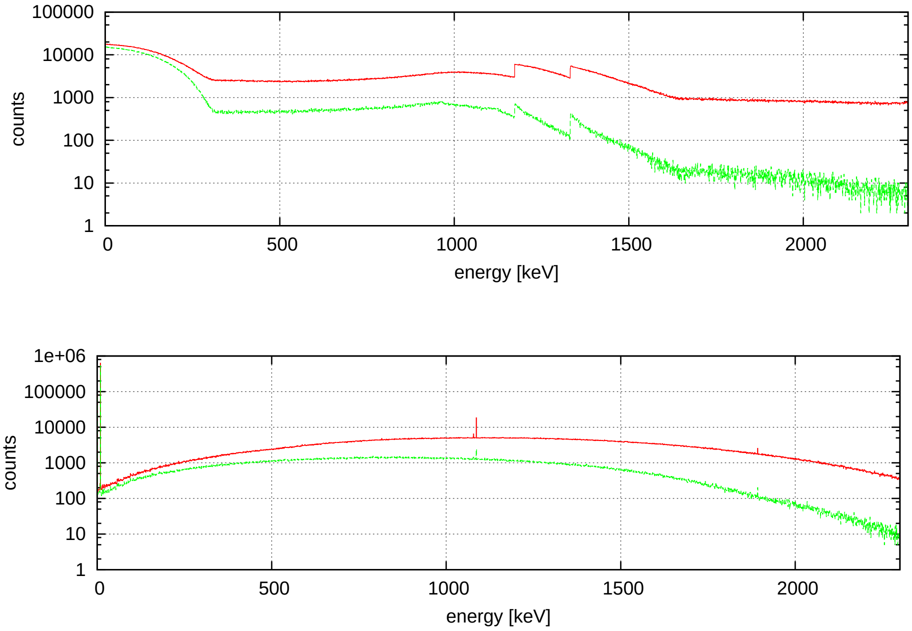

Figure 20: Simulated spectra of ^{60}Co (top) and ^{68}Ge (bottom) inside a BEGe detector, before (red line) and after (green line) the PSD cuts.

Tl-208 double escape peak (DEP) to 90%. The DEP has a topology which is similar to that of neutrinoless double beta decay events.

^{60}Co and ^{68}Ga are amongst the most challenging backgrounds in GERDA. The simulation shows that internal ^{60}Co background can be suppress by a factor of > 100 and ^{68}Ga by a factor 20 in the region of interest by pulse shape analysis alone using unsegmented p-type BEGe detectors. The ^{68}Ga decay can be further suppressed by about a factor 5 when tagging the 10.4 keV x-ray of the preceding ^{68}Ge decay.

It is noteworthy, that this is the first time that a PSD method is applied to simulated pulses in order to investigate and understand the discrimination performances for internal background sources.

11 Data management

At the last collaboration meeting in March 2010, the GERDA collaboration decided to set up a task group which takes care of all issues related to the data management and in particular the data quality.

The members of the new task group are: B. Schwingenheuer, L. Pandola, R. Brugnera, L. Baudis, C. Cattadori, M. Shirchenko, A. Bakalayrov, A. Vasenko, F. Cossavella, K. Zuber and P. Grabmayr (chair).

The duties include

- the definition of data storage locations during the data taking and for backup (raw data will be stored at LNGS, in Russia and in Germany),
- the definition of the method for combining the germanium data with the muon veto,
- the application of the correct calibration constants and the integration of the pulser data into the analysis,
- the definition of the frame work for the correlation to slow control data with germanium events,
- integration of sub-system monitoring into a common tool and the qualification of runs for further analysis.

The format of data storage has been agreed upon. The DAQ systems will store events as sequential files in individual formats. In parallel general information like the trigger conditions, start and end run times, and monitoring histograms will be stored for every run in the slow control database. The raw data are then copied to ROOT trees, called MGDO containers (see sec. 10), which are used for further analysis.

The blinding of the data could occur in the transition from raw data to the MGDO format.

12 Material screening

12.1 Radon measurements

Radon monitoring Since September 2009 the electrostatic radon monitor has been working at the GERDA site in hall A of LNGS. Within the next months it will be connected to the exhaust line of the GERDA cryogenic tank via a mass flow controller to measure the radon content of the gaseous Ar. Also, a dedicated emanation test of the GERDA commissioning lock is under discussion. The flow controller will split the argon flow and make it possible to bring only 6 liters per minute to the radon monitor. This process allows to maintain a gas exchange within 2 hours in our 711 liter radon monitor vessel.

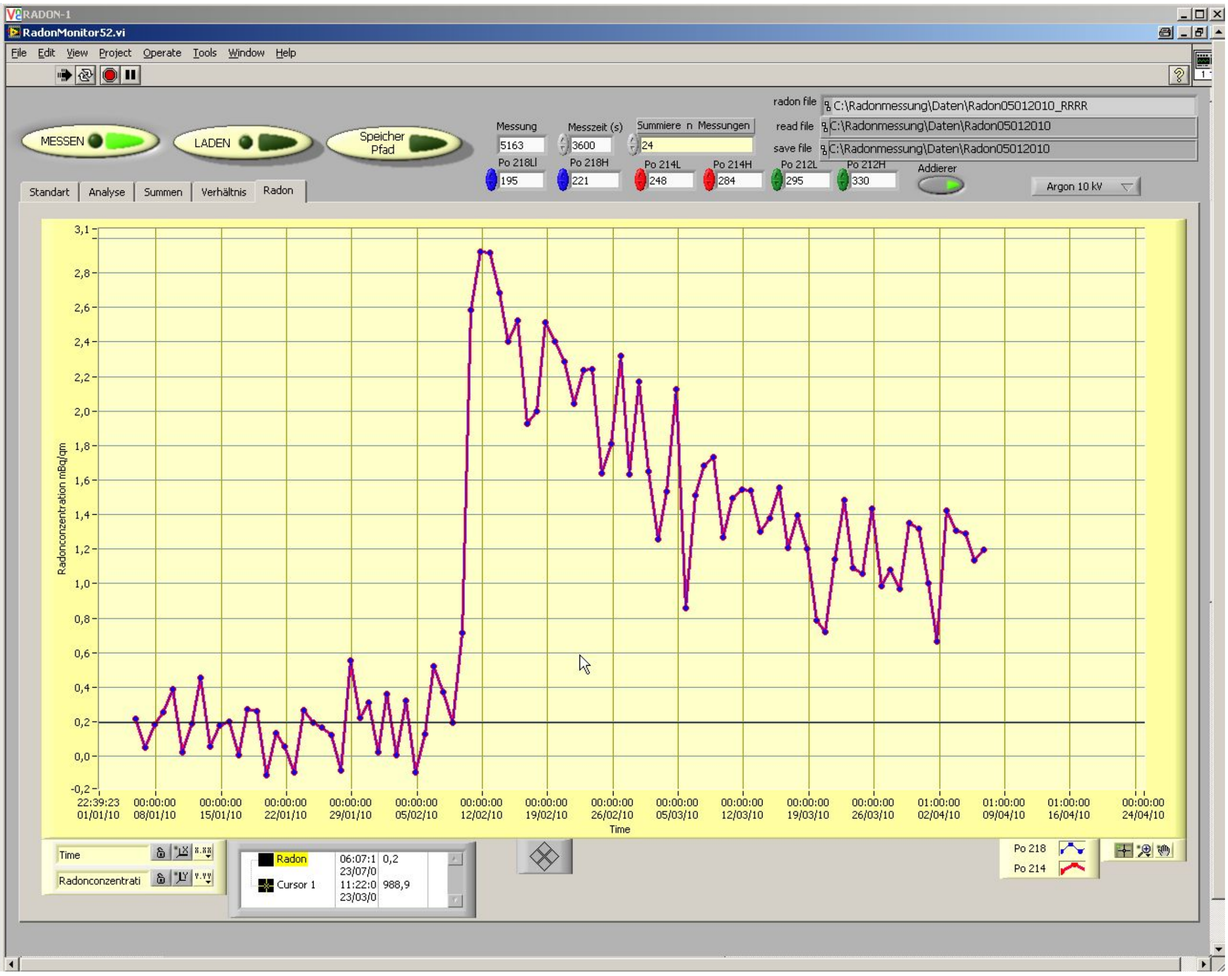

Figure 21: ^{222}Rn activity during $\sim$ 3 months of background data taking with the radon monitor installed at LNGS.

Under this condition a background of the radon monitor resulting from the emanation of the inner tank should stay below 15 μBq. For the estimated detection limit of about 70 μBq corresponding to two extra counts per day this emanation rate is sufficiently low.

In Figure 21 the loop-mode background measurement of the last month shows an activity of argon gas in the closed inner vessel including the inlet system of 0.2 ± 0.1 mBq/m^3. For the planed emanation test of the commissioning lock system an external pump and a ring copper line was mounted in Feb. 2010. After an initial increase the emanation of the whole system stabilized at the 1.2 mBq/m^3 level. With this background a measurement of the radon emanation of lock should be possible with an accuracy of $\pm$0.5 mBq.

Within the next month, the Labview software which calculates the radon concentration based on the ^{214}Po and ^{218}Po peak intensity will be updated. This update will make it possible to create a web site to read out the data and to set alarm levels via a web browser.

Radon emanation tests In the reporting period we have investigated the ^{222}Rn emanation of a meter drive system which provides information about the actual position of the detector string inside the GERDA cryostat. We investigated separately the reading head as well as the cable and the plug. Altogether the system contributes about 2 mBq to the ^{222}Rn emanation rate of the inner detector. The strongest contribution comes from the cable ((1.5±0.2) mBq) whereas the reading head and the plug only contribute (0.4±0.1) mBq and (0.2 ± 0.1) mBq, respectively.

12.2 Radon daughters on surfaces

The Rn daughter cleaning tests of different materials have been continued. In the last months we investigated the effect of Rn long-lived daughters removal from Ge surfaces. Two types of samples have been prepared: regular (optical quality) and high purity Ge in form of 50 mm diameter discs. Some of them, together with 2 liters of high purity distilled water, were artificially loaded with radon daughters. After 6 months of exposure optical quality Ge samples were etched by Canberra according to their standard procedure (applied to HPGe crystals). Screening with alpha, beta and gamma spectrometers before and after etching showed that ^{210}Po, ^{210}Bi and ^{210}Pb were removed with a very high efficiency (activity reduction factor of about 100). The same effect has been observed for high purity Ge surfaces. The other HPGe discs, not exposed to the ^{222}Rn source were processed in a solution prepared with the intensionally contaminated water. The idea behind this was to check if there will be a transfer of the isotopes from the solution to the metal surface. As a matter of fact such a transfer was observed. After etching the surface activities of all isotopes were significantly higher than before (increase up to 100 %). This shows that there is a surface cleanliness limit for the etched Ge crystals (given by the purity of the etchant) and that each detector should be always processed in a fresh solution in order to avoid its recontamination. In addition we found that compared to copper and steel, etching of germanium is very efficient for all the isotopes in question.

12.3 Gamma ray screening results

Again a large number of samples was investigated by gamma ray screening with low background Germanium detectors (see Table 3).

As mentioned earlier the radium problem with the PCBs could be solved by replacing the capacitors by special barium-free tantalum capacitors. Subsequently, the PCBs were further modified and screened in its current configuration. The achieved purity levels fulfill the specifications for phase I of GERDA. Also stainless steel parts were screened: The clamp rings and the tape will partly be in close proximity to the diodes, but since their masses are relatively small, they can be accepted. Another type of samples is related to the calibration sources. The tantalum absorber as well as the aluminum support shows relatively small activities. During normal data taking they are far away from the diodes, so their contribution is completely negligible.

Finally, the floor of the cleanroom above the GERDA water tank was investigated. It consists of a 2-component mixture of a resin and a filler. Both components were investigated individually as well as their final mixture. A high activity was obtained for the filler material (and of course for the final mixture) and a dedicated Monte Carlo campaign was carried out in order to estimate its background contribution. It was found that the water and argon shield between the clean room and the diodes is sufficient to reduce the contribution from the clean room floor to a negligible level.

	^{226}Ra	**^{228}Th**	**^{228}Ra**	**^{40}K**
Sample	**Activities [mBq/piece]**			
New pins for PCB	< 0.0038	0.003 ± 0.001	< 0.0062	0.02 ± 0.01
New modified PCBs	0.5 ± 0.1	0.3 ± 0.1	0.2 ± 0.1	3.2 ± 2.8
Old PCBs	6.3 ± 0.5	0.2 ± 0.1	0.2 ± 0.1	2.2 ± 0.7
	Mass activities [mBq/kg]			
Copper for PCB housing	< 1.8	< 2.2	< 1.3	< 22
SS bolts for LArGe	1.4 ± 0.3	3.6 ± 0.5	1.0 ± 0.5	6 ± 2
SS tape for position indicator	4 ± 1	3 ± 1	< 5	70 ± 20
SS clamp rings for cable chain	8.8 ± 1.5	7.7 ± 0.9	9.6 ± 1.1	32 ± 3
Ta absorber for calib. source	< 2.3	< 3.2	< 2.2	< 3.9
Al support for calib. source	< 13	490 ± 60	100 ± 25	< 65
Resin for clean room floor	820 ± 60	80 ± 30	80 ± 30	< 700
Filler for clean room floor	8900 ± 600	10000 ± 1000	8000 ± 1000	370 ± 40
Resin + filler for CR floor	9300 ± 400	9900 ± 600	9600 ± 500	340 ± 30

Table 3: Recent gamma ray screening results.

References

[1] http://ge-gate.lngs.infn.it/cryo/~gerda/cryo-s7.cgi

[2] http://ge-gate.lngs.infn.it/cryo/~gerda/actions.html

[3] http://ge-gate.lngs.infn.it/cryo/~gerda/pid.pdf

[4] M. Allardt et al, Progress report to the LNGS scientific committee, LNGS-EXP 33/05 add. 9/09, November 2009

[5] M. Knapp, PhD thesis 2009, Eberhard Karls Universität Tübingen

[6] M. Ballintijin, C. Loizides and C. Reed, Tree Analysis Modules, http://www.cmsaf.mit.edu/twiki/bin/view/Software/TAM

[7] Website: http://www.canberra.com/products/485.asp

[8] P. Medina, C. Santos, D. Villaume, "A simple method for the characterization of HPGe detectors", IEEE IMTC (2004).

[9] D. Budjas, M. Barnabe Heider, O. Chkvorets, S. Schönert and N. Khanbekov, "Pulse Shape Analysis with a Broad-Energy Germanium Detector for the GERDA experiment," arXiv:0812.1735 [nucl-ex].

[10] D. Budjas, "Germanium Detector Studies in the Framework of the GERDA experiment" Dissertation, University of Heidelberg (2009).

[11] M. Allardt et al., GERDA Progress report to the LNGS scient ific committee (Appendix) LNGS-EXP 33/05 add. 8/9 (April 2009).

[12] A.M. Bakalyarov et al., GERDA Progress report to the LNGS s cientific committee (Appendix) LNGS-EXP 33/05 add. 6/8 (April 2008).

[13] A.M. Bakalyarov et al., GERDA Progress report to the LNGS s cientific committee (Appendix) LNGS-EXP 33/05 add. 7/8 (October 2008).

[14] D. Lenz, dissertation, Technische Universität München, 2010

[15] I. Abt et al. arXiv:1004.0862v1